Food Research 7 (4) : 289 - 296 (August 2023)
Journal homepage: https://www.myfoodresearch.com

FOOD RESEARCH

FULL PAPER

The rapid detection of the infected seedlings of *Amorphophallus muelleri* using Visible Near-Infrared spectroscopy

Prastiwi, F.D., *Zahra, A.M., Rahayoe, S., Masithoh, R.E., Pahlawan, M.F.R., Nurrahmah, N.A. and Indrayanti, E.

Department of Agricultural and Biosystems Engineering, Faculty of Agricultural Technology, Universitas Gadjah Mada, Yogyakarta, Indonesia

Article history:
Received: 14 November 2021
Received in revised form: 4 January 2022
Accepted: 11 May 2022
Available Online: 28 August 2023

Keywords:
Amorphophallus muelleri,
Fungal infection,
Rapid detection,
Seedlings,
VIS-NIR spectroscopy

DOI:
https://doi.org/10.26656/fr.2017.7(4).907

Abstract

Porang (*Amorphophallus muelleri*) reproduces vegetatively using the bulbil, harvested during complete dormancy and spontaneous petiole detachment. However, the bulbils can be infected by fungi under certain harvesting and storage conditions, giving rise to non-uniform seed quality, and decreased plant growth and crop yields. This study aimed to develop a non-destructive technique for detecting infected and non-infected bulbils of porang using visible-near infrared (VIS-NIR). Additionally, 90 samples were used and measured five times in various conditions involving a calibrated set of spectra ranging from 450 – 950 nm and a binary label as the predictor (X) and criterion (Y), respectively, due to the qualitative nature of the data. The bulbil was determined quantitatively using VIS-NIR spectroscopy involving Principal Component Analysis (PCA), Partial Least Squares (PLS), Partial Least Squares-Discriminant Analysis (PLS-DA), and various pre-processing data. A PCA model was used to accurately determine the variance using two principal components (PC), including PLS and PLS-DA models. The PLS model was used to calculate the variance with accuracy and RMSE of 97.65% and 7.67%, respectively, while the variance was calculated with 100% accuracy using the PLS-DA model on all pre-processed data. Therefore, the narrow spectrum ranging between 450 and 950 nm enabled the implementation of low-cost assays, such as visible near-infrared spectroscopy, and the rapid detection of harmful contaminants during the chemical studies of fungal-infected bulbils.

1. Introduction

Porang (*Amorphophallus muelleri*) is a bulbous plant from the Araceae family. It produces a bulb and leaf tubers in its branching leaf stalks, used for vegetative propagation (Sari and Suhartati *et al*., 2015; Hidayah *et al*., 2018). The cultivation of Porang is essential due to its high glucomannan content, which serves as a valuable export commodity with numerous industrial applications. Subsequently, Porang products are exported in various forms, such as dried chips and flour, to specific regions in Asia, Australia, and several other countries in the European Union (Harmayani *et al*., 2014; Yanuriati *et al*., 2017).

Porang cultivation requires intensive management, including land preparation for seed planting and practices involving plant maintenance and tuber harvesting, which are well described in the Cultivation Operational Standard developed by the Ministry of Agriculture of the Republic of Indonesia (Soedarjo, 2020). However, there are risks associated with porang farming, such as disease infestation, specifically on the bulbil. The majority of Porang diseases are caused by fungi, such as *Sclerotium rolfsii*, *Phytophthora colocasiae*, *Fusarium solani*, *Fusarium oxysporum*, and *Botrytis cinerea* (Sakaroni *et al*., 2019; Soedarjo and Djufry, 2021). Porang trees produce new bulbils during their dormancy, which fall naturally around the mother plant as vegetative seeds (Utami, 2021) and are typically stored at room temperature before vegetative propagation. However, certain factors, such as high-water content, warm temperatures, and high humidity, can increase the spread of unexpected undetectable infections in newly fallen bulbils. Infections directly affect the quality of the bulbil, plant growth, and crop yield (Aini *et al*., 2020; Soedarjo and Djufry, 2021).

Several molecular approaches are frequently used in disease identification procedures, such as pathogenicity testing, ELISA (enzyme-linked immunosorbent assay), and RT-PCR (reverse transcriptase-polymerase chain

*Corresponding author.
Email: *aryanismutiazahra@ugm.ac.id*

eISSN: 2550-2166
Published by Rynnye Lyan Resources

reaction) (Babu *et al*., 2011; Aini *et al*., 2020). These methods require DNA sequencing, which is expensive, time-consuming, sophisticated, and destructive. Subsequently, disease-related concerns motivate efforts to examine young plant seeds to detect disease development in its early stages. The most suitable method to detect diseases is NIRS technology, a non-invasive, non-destructive, and rapid technique that does not require complex sample preparation. According to Canonical discriminant analysis, near-infrared spectroscopy at a range of 900 – 2600 nm has been successfully used to detect zebra chip disease in potatoes at an early stage, with an overall classification accuracy of 97.25 – 98.35% (Liang *et al*., 2018). Furthermore, visible-near infrared (VIS-NIR) has been used to detect black spots on potatoes, with a correct classification rate of over 94% based on Partial Least Squares-Discriminant Analysis (PLS-DA) (López-Maestresalas *et al*., 2016). The early detection of frog skin disease was also detected in cassava, with an accuracy greater than 80%, achieved through High Dimensional Discriminant Analysis and Partial Least Squares (PLS) methods (Freitas *et al*., 2020).

Another method employed in the early detection of symptoms involves using near-infrared spectroscopy (NIRS), an iterative and indirect procedure. The NIRS method could determine the light-reflected spectrum based on the plant species, its internal characteristics, and biochemical activity. The progression of an epidemic involves metabolic and physical changes caused by pathogens, which can affect optical absorption and cause variations in reflectance (Freitas *et al*., 2020). Therefore, this study aimed to investigate the rapid detection of fungi using VIS-NIR in porang bulbils, which caused a non-uniform quality in the plant. The study procedures included the determination of the wavelength associated with the fungal-infected bulbils, classifying the non-infected bulbils as normal porang seeds, comparing the spectral pattern, and developing a classification model to identify non-infected and infected bulbils.

2. Materials and methods

2.1 Sample preparation

The study included ninety samples, classified into infected and non-infected seeds. The porang bulbils were harvested during the last quarter of the tree's vegetative phase and stored for approximately one month before use with initial moisture content, weight, and area of 75% (wet basis), 5.00 g, and 210 cm^2, respectively.

2.2 Spectra acquisitions

Four hundred fifty reflectance spectra (350 – 1000 nm) were obtained from 90 samples, measured five times in different positions using a VIS-NIR spectrometer (Flame T-VIS-NIR Ocean Optics) and a spectra acquisition setup, as shown in Figures 1 and 2. The spectrum was measured using a fiber-optic probe (QR400-7-VIS-NIR Ocean Optics) and a tungsten halogen lamp (350 – 2400 nm, HL-2000-HP-FHSA Ocean Optics). The spectra were collected at a distance of 0.5 cm between the sample and the probe. An average of 100 scans and an integration time of 100 ms were used to collect spectra in a boxcar width of 1. According to previous studies, a distance of 0 between the sample and the probe produces the worst model performance since a greater distance between the sample and the probe can reduce the energy used before it reaches the samples (Pahlawan *et al.,* 2021). Subsequently, the white reference was measured with a ceramic diffuse reflectance standard (WS-1, Ocean Optics, USA) during the dark reference with a blocked light source. The measuring instruments were re-calibrated after the successive assay of ten samples.

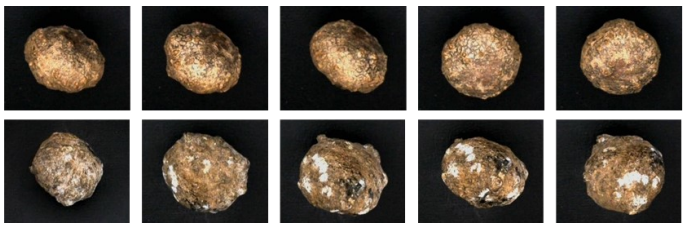

Figure 1. Infected and non-infected *Amorphophallus muelleri* bulbil with five different positions.

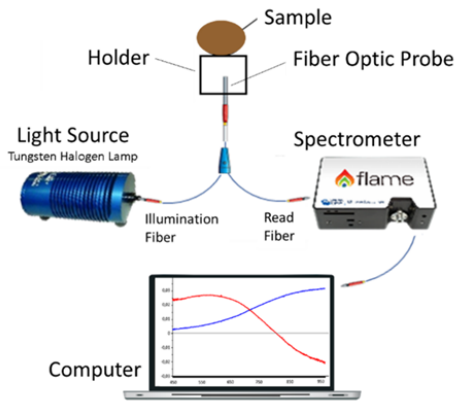

Figure 2. Spectra acquisition setup.

2.3 Multivariate analysis

All spectral data were compiled, and only spectra within the 450 – 950 nm range were used to minimize noise, which was finally resolved using MS Excel® at the preliminary stage. The spectral wavelength between 450 – 950 nm was inputted into the Unscrambler® X software application (CAMO, Oslo, Norway). The raw spectra and pre-processed data are processed to improve model performance using baseline correction, the Standard Normal Variate (SNV), De-trending, and Multiple Scatter Correction (MSC) methods. The

https://doi.org/10.26656/fr.2017.7(4).907

samples were divided into two groups based on calibration (3/4 data or 270 spectra) and prediction (1/4 data or 180 spectra). The analytical methods used in this study were Principal Component Analysis (PCA), PLS, and PLS-DA. PCA is an unsupervised method that can reduce dimension, recognize patterns, and identify outliers, while PLS is a supervised method for developing a quantitative model. The sample was binary labelled based on the fungal infection to develop a quantitative parameter (non-infected and infected seeds labelled as 1 and 0, respectively). The calibration set was used to develop a PLS calibration model using the spectra as the predictor (X) and the binary label as the criterion (Y). The proposed models were validated using prediction sets. PLS-DA is an extension of PLS that involves the conversion of the PLS value from the decimal form into a binary label, which is then analyzed using the specified threshold value, as shown in Table 1 (Szyman'ska *et al*., 2012). The predicted PLS values greater than 0.5 were rounded to 1, while values less than 0.5 were rounded to 0.

Table 1. Discriminant analysis parameter of *Amorphophallus muelleri* bulbil.

Case	Non-infected		Class	Parameter
	True	Predicted		
A	1	0.55	1	True non-infected (TN)
B	1	0.49	0	False infected (FI)
C	0	0.37	0	True infected (TI)
D	0	0.67	1	False non-infected (FN)

2.4 Evaluation of calibration and validation results

PCA involves the development of axes by linearly combining spectral variables known as principal components (PC), data predictors based on the most significant variance. Therefore, an A-line containing more fundamental components will have a higher variance and more data points. Another common technique used in revealing hidden patterns in spectral data was the CA (Wu *et al.*, 2020).

The coefficient of determination (R^2) and Root Mean Square Error was used to examine the PLS calibration and validation findings (RMSE). The coefficient of determination represented the independent contribution to the dependent variable. Subsequently, the RMSE was calculated using the estimated and actual values based on the highest R2 and lowest RMSE to yield a reliable model (Tamburini *et al.*, 2016; Masithoh *et al.*, 2020).

The calibration and validation results of PLS-DA were evaluated using Model Accuracy (Acc) and Model Reliability (Rel). PLS-DA consisted of PLS regression values and a dependent variable y representing the class membership, where the best model had the highest Acc and Rel values (Pahlawan *et al.*, 2021). PLS-DA was an excellent method for determining the linear correlation between spectral and categorical variables in numeric form. Specifically, the PLS-DA algorithm turns spectral data into latent regressors that retain variation information while optimizing correlation with the categorical variable in contrast to PCA (Wu *et al.*, 2020). The following equation can be used to calculate the R^2, RMSE, Acc, and Rel values.

$$R = \left(\frac{(Yref - \bar{Y}ref)(Ypred - \bar{Y}pred)}{\sqrt{(Yref - \bar{Y}ref)^2 \sum(Ypred - \bar{Y}pred)}}\right)^2 \quad (1)$$

$$RMSE = \frac{\sqrt{\sum(Ypred - Yref)}}{n} \quad (2)$$

$$Acc = \frac{TN+TI}{TN+TI+FI+FN} \times 100\% \quad (3)$$

$$Rel = \left(\frac{TN}{TN+FI} + \frac{TI}{TI+FN} - 1\right) \times 100\% \quad (4)$$

3. Results and discussion

3.1 Visible-near infrared spectroscopy of Amorphophallus muelleri bulbil

The VIS-NIR raw spectrum of the infected and uninfected bulbils is shown in Figure 3, and the reflectance graph shows some of the content found in the porang bulbil. The use of VIS-NIR and chemometric methods for early detection is a prominent technique used in the non-destructive analysis of various biological materials, with the advantage of greater sensitivity than using only the naked eye (Azmi *et al*., 2021). VIS-NIR can detect fungi and identify infected and non-infected seeds (del Fiore *et al*., 2010; Shahin *et al*., 2014). The spectra showed similar characteristics between 450 and 550 nm, corresponding to chlorophyll, carotenoid, and anthocyanin pigments (Shahin *et al*., 2014; Masithoh *et al*., 2021). Also, there was a correlation between the variation in the spectrum and the chlorophyll content at the peak of the wavelength ranging between 640-700 nm (Cortés *et al*., 2016; Pahlawan *et al*., 2021). There was an increase in the spectrum value between 700 and 950 nm, as well as a third or fourth overtone of the -CH and -OH stretching, which corresponded to the absorption area of water and sugar groups (Shahin *et al*., 2014; Phetpan *et al*., 2018; Wati *et al*., 2021).

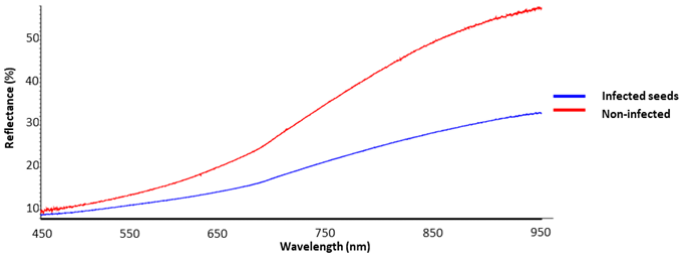

Figure 3. Visible-near infrared reflectance spectra of infected and non-infected bulbil

Fungal infections caused a lower reflectance

https://doi.org/10.26656/fr.2017.7(4).907

spectrum in bulbils than in non-infected bulbils. The VIS-NIR data retrieval method used in this study detected fungal infections at a 450 – 1000 nm wavelength range, consistent with a previous study by Shahin *et al*. (2014). The spectra of 450–950 nm and 1000–2000 nm were used to evaluate the growth rates and predict fungal damage on wheat germ, specifically Fusarium species. According to previous reports, fungal damage primarily affects the intensity and slope changes in the 450 – 950 nm spectral range. According to Del Fiore *et al*. (2010), there were spectrum changes caused by *Aspergillus* on artificially inoculated maize kernels in 400 – 1000 nm spectral region.

3.2 Calibration and validation using the principal component analysis method

The qualitative analysis of VIS-NIR using PCA was conducted to identify non-infected and infected porang bulbils. It was observed that there was an increased absorbance in the spectral features towards the near-infrared visible region of 550 nm in the infected bulbils, while the non-infected bulbils showed a decreased absorbance. The spectrum intersection between 650 and 750 nm is the most significant classification feature, as shown in Figure 4. Del Fiore *et al*. (2010) reported using HSI on corn kernels inoculated with several species of Aspergillus at a 400–1000 nm wavelength. The results of PCA based on the Discriminant Analysis showed that fungal activity caused significant spectrum changes. The spectral characteristics of the fungus were implicated in the spectral difference between the contaminated and uncontaminated maize at wavelengths less than 700 nm. Furthermore, the wavelengths with the highest correlation values were 535 and 945 nm based on PCA's first three principal components, which showed *A. flavus* activities.

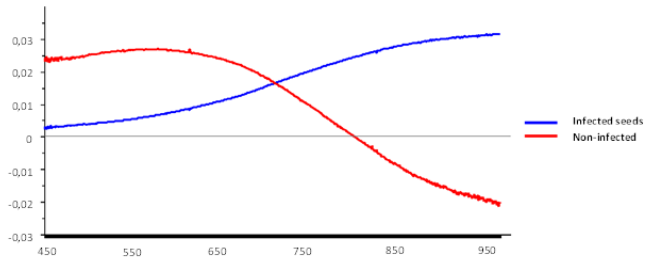

Figure 4. Loadings plot of principal component analysis of infected and non-infected bulbil.

Figure 5 shows the scores plot for the first two PC from PCA on the NIR spectra of porang bulbil. PCA explained 100% of the total variance, where PC1 and PC2 accounted for 97% and 3%, respectively. The non-infected porang seeds were spread across quadrants 2, 3, and 4 in the graph. Quadrant 4 was mainly based on the positive and negative values of PC1 and PC2, respectively. In contrast, infected porang seeds tend to separate in quadrants 1, 2, and 3 of the graphs, where quadrant 1 was dominantly based on a negative value of PC1 and a positive value of PC2. Manual calculations were also performed based on the results of PCA plot scores by drawing the closest line separating infected and non-infected seeds. The manual calculation results showed that 1% of infected seeds fall into the non-infected group, while 22% of non-infected seeds fall into the infected group. PCA showed the discriminative power of healthy and infected rice kernels for laboratory-inoculated and field-inoculated rice kernels using NIR-HSI with spectral variations of about 99.76%. The study concluded that PCA discrimination should be reserved for on-trend discrimination and substituted with a more precise quantitative analysis (Wu *et al*., 2020).

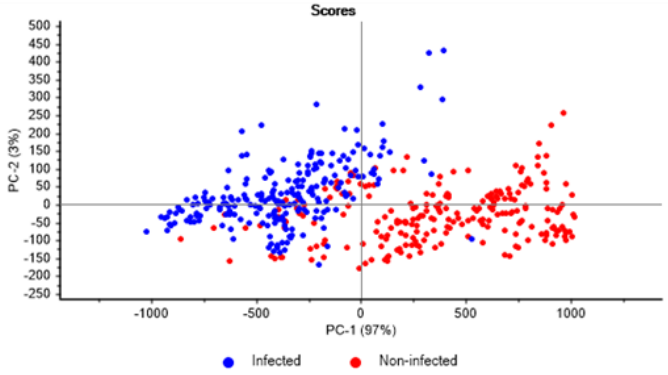

Figure 5. Principal component analysis scores plot of infected and non-infected bulbil.

3.3 Calibration and validation using partial least squares method

Table 2 shows the calibration and validation results using the PLS technique. The most accurate prediction model can be determined using statistical indicators, such as R^2, SEC, SEP, and root mean standard error (RMSEP) (Tamburini *et al*., 2016; Masithoh *et al*., 2020). The coefficient of determination (R^2C) was about 100% after the De-trending pre-processing, while the Root Mean Square Error (RMSE) was low. The R^2C score for De-trending was 97.65%, indicating that this model can accurately identify infected and non-infected bulbils.

Figure 6 shows the linear regression coefficient of PLS for wavelengths ranging from 450 – 940 nm, which involved irregular spectra, with 490, 660, and 715 nm peaks and valleys of 559 and 685 nm. The peak wavelength of 490 nm corresponded to the yellow colour of bulbils, which is associated with the beta-carotene content (López-Maestresalas *et al*., 2016). The presence of chlorophyll was detected by the peak at 640-700 nm (Cortés *et al*., 2016), while water absorption occurred at 760 nm in the deep 720 – 1000 nm range (Min *et al*.,

https://doi.org/10.26656/fr.2017.7(4).907

Table 2. PLS model performances.

Pre-processing Techniques	Calibration		Validation		Prediction	
	R^2C	RMSEC	R^2V	RMSEV	R^2P	RMSEP
Ori	90.99%	15.01%	88.92%	16.70%	90.93%	15.06%
De Trend	97.65%	7.67%	95.33%	10.85%	94.79%	11.41%
SNV	94.85%	11.34%	92.20%	14.01%	91.72%	14.39%
MSC	95.10%	11.07%	92.57%	13.68%	91.86%	14.27%
Baseline	93.77%	12.47%	91.85%	14.33%	89.83%	15.95%
Area N	93.43%	12.82%	91.52%	14.61%	90.95%	15.04%
UV N	90.28%	15.59%	88.28%	17.18%	88.26%	17.13%
Mean N	93.43%	12.82%	91.82%	14.61%	90.95%	15.04%
Max N	92.68%	13.53%	90.99%	15.07%	87.67%	17.56%
Range N	91.78%	14.33%	90.15%	15.75%	84.74%	19.53%

2006). Other studies successfully reported using the PLS regression model to detect nine classes of fungal infections in wheat grains at the VIS-NIR wavelength range of 450 – 900 nm (Shahin *et al*., 2014). However, pre-treatment with PLS based on normalization and SNV or mean centering can produce the lowest RMSE of less than 1 and 96% accuracy due to colour changes from fungal attacks. According to Chakraborty *et al*. (2021), the PLS model and VIS-NIR in the 400 – 1000 nm spectral range produced good PLS results in the early detection of *Aspergillus flavus* in corn kernels, as well as predicting the actual content of aflatoxin B1 at R^2C and R^2V values of 0.873 and 0.820, respectively.

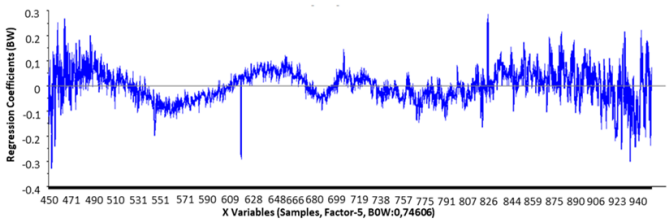

Figure 6. Regression coefficients (BW) of PLS.

The calibration and validation results were also graphically displayed in Figure 7. Binary discriminators were used to differentiate the two bulbil states, but the data was still inaccurate. The data obtained from the PLS model was converted to binary labels using PLS-DA since the results were in decimal values and unreliable when applied to categorical data. Therefore, PLS prediction values greater than 0.5 were labelled 1 (non-infected seed), while those less than 0.5 were labelled 0 (infected seed).

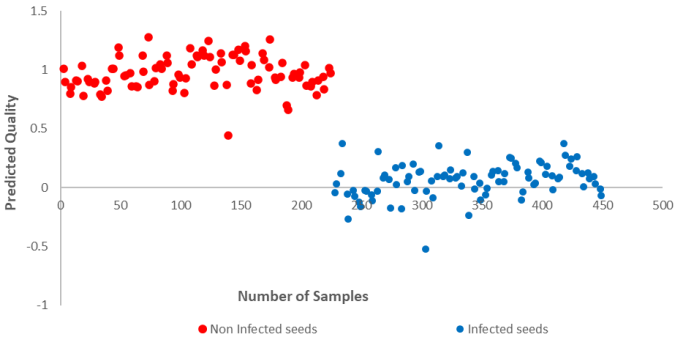

Figure 7. Classification of infected and non-infected bulbil using the PLS model.

3.4 Calibration and validation using the partial least squares-discriminant analysis method

The calibration and validation results for the PLS-DA method are shown in Table 3. The results showed that PLS-DA poses a linear constraint on the PLS regression, where the regression model visualizes the predicted (y) and observed (x) variables as projections (Kalogiouri, 2020). Subsequently, matrix analysis can be used to evaluate the performance of the PLS-DA model in determining numerical superiority based on accuracy, sensitivity, parameters, and error rate (da Conceição *et al*., 2021). Linear Discriminant Analysis (LDA) was

Table 3. PLS-DA model performances.

Pre-processing Techniques	Calibration		Validation		Prediction	
	Acc	Rel	Acc	Rel	Acc	Rel
Ori	100%	100%	100%	100%	99%	99%
De Trend	100%	100%	100%	100%	99%	99%
SNV	100%	100%	100%	100%	100%	100%
MSC	100%	100%	100%	100%	100%	100%
Baseline	100%	100%	100%	99%	99%	99%
Area N	100%	100%	100%	100%	99%	99%
UV N	100%	99%	99%	99%	99%	98%
Mean N	100%	100%	100%	100%	99%	99%
Max N	100%	100%	100%	100%	99%	99%
Range N	100%	100%	100%	100%	99%	99%

https://doi.org/10.26656/fr.2017.7(4).907

primarily used to establish the relationship between the X matrix of predictors and the Y matrix of indicators to determine class membership based on Canonical Correlation Analysis (CCA). However, CCA results were substituted for PLS results to form the PLS-DA since the study aimed to examine highly correlated predictors. The predicted values were not absolute in binary form and did not correspond with the entire real axis, limiting their use in class membership's direct interpretation (Stocchero *et al*., 2021).

The data for infected porang bulbil was plotted against non-infected ones using a binary label in Figure 8. The infection rates were not uniformly distributed since the bulbils used were infected in the field and stored. Most bulbils had an infection rate of less than or equal to zero, and only a few had a high infection rate. However, the PLS-DA model accurately and reliably identified the infected and non-infected porang seeds on all original spectra and pre-processed data at 98–100% accuracy and reliability. Another study determined the presence of fusarium damage in wheat kernels at 90% accuracy and 9% false positives. The spectral region between 500 and 700 nm can also detect damage with mild to severe symptoms (Shahin, 2012). The PLS-DA model was used in another study to detect *A. flavus* on corn kernels early at a maximum PLS-DA accuracy of 94.7% using SNV pre-processing (Chakraborty *et al*., 2021).

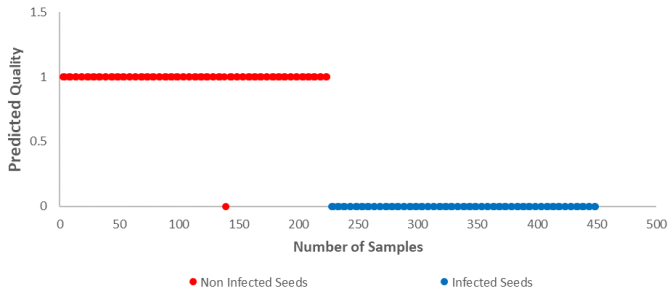

Figure 8. Classification of infected and non-infected bulbil using the PLS-DA model.

Conflict of interest

The authors declare no conflict of interest.

Acknowledgments

Innovative Research Grants 2021, Faculty of Agricultural Technology, Universitas Gadjah Mada, supported and sponsored this work with contract number 2719/UN1/FTP.1.3/SET-D/KU/2021.

References

Aini, A.N., Azrianingsih, R. and Mustofa, I. (2020). Identification of potential pathogen bacteria causing tuber rot in Porang (*Amorphophallus muelleri* blume). *Journal of Tropical Life Science*, 10(2), 99–104. https://doi.org/10.11594/jtls.10.02.02

Azmi, M.F.I., Jamaludin, D., Abd. Aziz, S., Yusof, Y.A. and Mustafah, A.M. (2021). Adulterated stingless bee honey identification using VIS-NIR spectroscopy technique. *Food Research,* 5(Suppl. 1), 85 – 93. https://doi.org/10.26656/fr.2017.5(S1).035

Babu, B., Hegde, V., Makeshkumar, T. and Jeeva, M.L. (2011). Molecular detection and identification of Dasheen mosaic virus infecting *Amorphophallus paeoniifolius*. *Archives of Phytopathology and Plant Protection*, 44(13), 1248–1260. https://doi.org/10.1080/03235408.2010.490398

Chakraborty, S.K., Mahanti, N.K., Mansuri, S.M., Tripathi, M.K., Kotwaliwale, N. and Jayas, D.S. (2021). Non-destructive classification and prediction of aflatoxin-B1 concentration in maize kernels using Vis–NIR (400–1000 nm) hyperspectral imaging. *Journal of Food Science and Technology*, 58(2), 437–450. https://doi.org/10.1007/s13197-020-04552-w

Cortés, V., Ortiz, C., Aleixos, N., Blasco, J., Cubero, S. and Talens, P. (2016). A new internal quality index for mango and its prediction by external visible and near-infrared reflection spectroscopy. *Postharvest Biology and Technology*, 118, 148–158. https://doi.org/10.1016/j.postharvbio.2016.04.011

da Conceição, R.R.P., Simeone, M.L.F., Queiroz, V.A.V., de Medeiros, E.P., de Araújo, J.B., Coutinho, W.M., da Silva, D.D., de Araújo Miguel, R., de Paula Lana, U.G. and de Resende Stoianoff, M.A. (2021). Application of near-infrared hyperspectral (NIR) images combined with multivariate image analysis in the differentiation of two mycotoxicogenic Fusarium species associated with maize. *Food Chemistry*, 344, 128615. https://doi.org/10.1016/j.foodchem.2020.128615

del Fiore, A., Reverberi, M., Ricelli, A., Pinzari, F., Serranti, S., Fabbri, A.A., Bonifazi, G. and Fanelli, C. (2010). Early detection of toxigenic fungi on maize by hyperspectral imaging analysis. *International Journal of Food Microbiology*, 144(1), 64–71. https://doi.org/10.1016/j.ijfoodmicro.2010.08.001

Freitas, E.L., Brito, A.C., de Oliveira, S.A.S. and de Oliveira, E.J. (2020). Early diagnosis of cassava frog skin disease in powdered tissue samples using near-infrared spectroscopy. *European Journal of Plant Pathology*, 156(2), 547–558. https://doi.org/10.1007/s10658-019-01904-x

Harmayani, E., Aprilia, V. and Marsono, Y. (2014). Characterization of glucomannan from *Amorphophallus oncophyllus* and its prebiotic activity in vivo. *Carbohydrate Polymers*, 112, 475–

479. https://doi.org/10.1016/j.carbpol.2014.06.019

Hidayah, N., Rahmad Suhartanto, M. and Santosa, D.E. (2018). Growth and Production Iles-iles (*Amorphophallus muelleri* Blume) from Different of Cultivation Techniques. In *Buletin Agrohorti*, 6(3), 405–411. https://doi.org/10.29244/agrob.v6i3.21109

Kalogiouri, N.P. and Samanidou, V.F. (2020). Liquid chromatographic methods coupled to chemometrics: a short review to present the key workflow for the investigation of wine phenolic composition as it is affected by environmental factors. *Environmental Science and Pollution Research International,* 28 (42), 59150–59164. https://doi.org/10.1007/s11356-020-09681-5

Liang, P.S., Haff, R.P., Hua, S.S.T., Munyaneza, J.E., Mustafa, T. and Sarreal, S.B.L. (2018). Non-destructive detection of zebra chip disease in potatoes using near-infrared spectroscopy. *Biosystems Engineering*, 166, 161–169. https://doi.org/10.1016/j.biosystemseng.2017.11.019

López-Maestresalas, A., Keresztes, J.C., Goodarzi, M., Arazuri, S., Jarén, C. and Saeys, W. (2016). Non-destructive detection of blackspot in potatoes by Vis-NIR and SWIR hyperspectral imaging. *Food Control*, 70, 229–241. https://doi.org/10.1016/j.foodcont.2016.06.001

Masithoh, R.E., Lohumi, S., Yoon, W.S., Amanah, H.Z. and Cho, B.K. (2020). Development of multi-product calibration models of various root and tuber powders by fourier transform near infra-red (FT-NIR) spectroscopy for the quantification of polysaccharide contents. *Heliyon*, 6(10), e05099. https://doi.org/10.1016/j.heliyon.2020.e05099

Masithoh, R.E., Pahlawan, M.F.R. and Wati, R.K. (2021). Non-destructive determination of SSC and pH of banana using a modular VIS-NIR spectroscopy: Comparison of Partial Least Square (PLS) and Principal Component Regression (PCR). *IOP Conference Series: Earth and Environmental Science*, 752(1), 012047. https://doi.org/10.1088/1755-1315/752/1/012047

Min, M., Lee, W.S., Kim, Y.H. and Bucklin, R.A. (2006). Non-destructive Detection of Nitrogen in Chinese Cabbage Leaves Using VIS-NIR Spectroscopy. *Hortscience*, 41(1), 162–166. https://doi.org/10.21273/HORTSCI.41.1.162

Pahlawan, M.F.R., Wati, R.K. and Masithoh, R.E. (2021). Development of a low-cost modular VIS-NIR spectroscopy for predicting soluble solid content of banana. *IOP Conference Series: Earth and Environmental Science*, 644(1), 012047. https://doi.org/10.1088/1755-1315/644/1/012047

Phetpan, K., Udompetaikul, V. and Sirisomboon, P. (2018). An online visible and near-infrared spectroscopic technique for the real-time evaluation of the soluble solids content of sugarcane billets on an elevator conveyor. *Computers and Electronics in Agriculture*, 154, 460–466. https://doi.org/10.1016/j.compag.2018.09.033

Sakaroni, R., Suharjono, S. and Azrianingsih, R. (2019). Identification of potential pathogen fungi which cause rotten on Porang (*Amorphophallus muelleri* Blume) tubers. *AIP Conference Proceedings*, 2120, 080010. https://doi.org/10.1063/1.5115748

Sari, R. and Suhartati. (2015). Prospects of Cultivation of Porang Plants: Prospects of Cultivation as one of the Agroforestry Systems. *Teknis EBONI*, 12(2), 97-110.

Shahin, M.A. and Symons, S.J. (2012). Detection of *Fusarium* damage in Canadian wheat using visible/near-infrared hyperspectral imaging. *Journal of Food Measurement and Characterization*, 6(1–4), 3–11. https://doi.org/10.1007/s11694-012-9126-z

Shahin, M.A., Symons, S.J. and Hatcher, D.W. (2014). Quantification of Mildew Damage in Soft Red Winter Wheat Based on Spectral Characteristics of Bulk Samples: A Comparison of Visible-Near-Infrared Imaging and Near-Infrared Spectroscopy. *Food and Bioprocess Technology*, 7(1), 224–234. https://doi.org/10.1007/s11947-012-1046-8

Soedarjo, M. and Djufry, F. (2021). Identified diseases would threaten on the expansion of *Amorphophallus muellery* Blume cultivation in Indonesia. *IOP Conference Series: Earth and Environmental Science*, 648(1), 012043. https://doi.org/10.1088/1755-1315/648/1/012043

Soedarjo, M. (2020). Growth Response of Porang (*Amorphophallus muelleri* Blume) Grown with Different Sizes of Bulbils on Saline Soil. *International Journal of Research Studies in Agricultural Sciences*, 6(4), 8–16. https://doi.org/10.20431/2454-6224.0604002

Stocchero, M., De Nardi, M. and Scarpa, B. (2021). PLS for classification. *Chemometrics and Intelligent Laboratory Systems*, 216, 104374. https://doi.org/10.1016/j.chemolab.2021.104374

Szyman´ska, E., Saccenti, E., Smilde, A.A. and Westerhuis, J.A. (2012). Double-check: validation of diagnostic statistics for PLS-DA models in metabolomics studies. *Metabolomics,* 8, 3–16. https://doi.org/10.1007/s11306-011-0330-3

Tamburini, E., Mamolini, E., De Bastiani, M. and Marchetti, M.G. (2016). Quantitative determination of *Fusarium proliferatum* concentration in intact garlic cloves using near-infrared spectroscopy.

Sensors, 16(7), 1099. https://doi.org/10.3390/s16071099

Utami, M.A.W. (2021). Economic prospects for porang plant development during the COVID-19 pandemic. *Journal Viabel Pertanian*, 15(1), 72–82. https://doi.org/10.35457/viabel.v15i1.1486

Wati, R.K., Pahlawan, M.F.R. and Masithoh, R.E. (2021). Development of calibration model for pH content of intact tomatoes using a low-cost VIS-NIR spectroscopy. *IOP Conference Series: Earth and Environmental Science*, 686(1), 012049. https://doi.org/10.1088/1755-1315/686/1/012049

Wu, N., Jiang, H., Bao, Y., Zhang, C., Zhang, J., Song, W., Zhao, Y., Mi, C., He, Y. and Liu, F. (2020). Practicability investigation of using near-infrared hyperspectral imaging to detect rice kernels infected with rice false smut in different conditions. *Sensors and Actuators, B: Chemical*, 308, 127696. https://doi.org/10.1016/j.snb.2020.127696

Yanuriati, A., Marseno, D.W., Rochmadi and Harmayani, E. (2017). Characteristics of glucomannan isolated from fresh tuber of Porang *(Amorphophallus muelleri* Blume). *Carbohydrate Polymers*, 156, 56–63. https://doi.org/10.1016/j.carbpol.2016.08.080

